Polymer Journal, Vol. 36, No. 10, pp. 830—840 (2004)

Solid-State ^{13}C NMR Analysis of the Crystalline–Noncrystalline Structure and Chain Conformation of Thermotropic Liquid Crystalline Polyester

Miwa MURAKAMI, Hiroyuki ISHIDA, Hironori KAJI, Fumitaka HORII,† Masatoshi TOKITA,* and Junji WATANABE*

Institute for Chemical Research, Kyoto University, Uji 611-0011, Japan
**Department of Organic and Polymer Materials Chemistry, Tokyo Institute of Technology, Ookayama, Meguro-ku, Tokyo 152-8522, Japan*

(Received May 6, 2004; Accepted June 18, 2004; Published October 15, 2004)

ABSTRACT: The crystalline–noncrystalline structure and chain conformation of thermotropic liquid crystalline polyester (BB-8), composed of mesogenic biphenyl and spacer CH_2 sequence units, have been characterized by high-resolution solid-state ^{13}C NMR spectroscopy. The sample was crystallized by cooling from the melt through the smectic A phase. ^{13}C spin–lattice relaxation measurements reveal that all resonance lines contain three components with different T_1^C values of 200–430, 9–38, and 0.4–5.5 s, which correspond to the crystalline, medium, and noncrystalline components, respectively. The high-resolution ^{13}C NMR spectrum for each component is selectively recorded by utilizing the difference in T_1^C and conformation of the spacer CH_2 sequences of each component is evaluated by considering the *γ-gauche* effect on ^{13}C chemical shift values. The noncrystalline component is found to adopt a characteristic conformation *xttttttx* in which the *trans–gauche* exchange conformations (*x*) are introduced at both ends of the CH_2 sequence, whereas the all-*trans* conformation *ttttttt* is allowable for the crystalline and medium components. ^{13}C chemical shift anisotropy spectra of the respective carbons are obtained by the two-dimensional magic angle turning method to examine molecular motion of the mesogen and spacer units. The mesogenic phenylene units undergo rapid fluctuation around the bond axis of the units in the medium and noncrystalline components while the crystalline component is highly restricted in such molecular motion. On the basis of these results, a molecular motion model is proposed for the noncrystalline component, which corresponds to the supercooled smectic A phase, for the BB-8 sample.
[DOI 10.1295/polymj.36.830]

KEY WORDS Liquid Crystalline Polymer / Polyester / Solid-State ^{13}C NMR / Conformation / Co-planarity / Molecular Motion /

Many different main-chain thermotropic liquid crystalline (LC) polymers have been developed and their phase transition behavior and structures in different levels have extensively been investigated by calorimetry, microscopy, diffractometry, spectroscopy, and so on.[1–5] We have systematically investigated the phase transition behavior and the crystalline–noncrystalline structure, particularly focusing attention on the conformation and dynamics of the mesogen and spacer units, for main-chain thermotropic LC polyurethane (UDMB-10) and polyether (EDMB-10) (Scheme 1) mainly by solid-state ^{13}C NMR spectroscopy.[6,7] These LC polymers have similar chemical structures composed of 3,3′-dimethyl-4,4′-biphenyl units as mesogen and 10 CH_2 sequences as spacer. The thermal analysis and optical polarizing microscopic observation of the polymers revealed that the nematic phase appears in a somewhat narrow temperature region when cooled from the melt or heated from the crystalline phase.[6–10] ^{13}C spin–lattice relaxation measurements for the samples crystallized by cooling from the melt through the nematic phase indicated three components with different molecular mobilities which are assigned to the crystalline, medium, and noncrystalline components.[6–8,10] By line shape analysis for the respective components and the evaluation of the ^{13}C chemical shifts in terms of the *γ-gauche* effect, it was found that the spacer CH_2 sequences adopt the characteristic conformation (*ttxtxtxtt*) in the noncrystalline component for UDMB-10, whereas

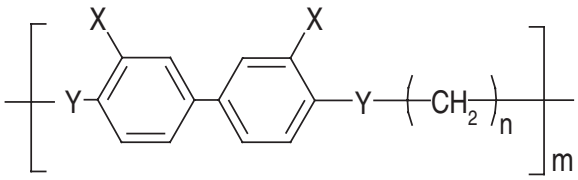

BB-8: X = H, Y= COO, n= 8
EDMB-10: X= CH_3, Y= O, n=10
UDMB-10: X= CH_3, Y=NHCOO, n=10

Scheme 1.

†To whom correspondence should be addressed (E-mail: horii@scl.kyoto-u.ac.jp).

both the crystalline and medium components simply take the planar zigzag conformation (*tttttttt*).[6,8] Here, the *trans* and the *trans–gauche* exchange conformations are designated by *t* and *x*, respectively. Similar characterization of EDMB-10 also revealed that the CH_2 sequences of the crystalline and medium components take the alternate *txtxtxtxt* conformation while the *xxxxxxxxx* conformation is allowed for the noncrystalline component as with the case in the melt.[7,8] These results show the usefulness of the solid-state ^{13}C NMR analysis to characterize the spacer conformation of each component involved in different thermotropic LC polymers.

Main-chain thermotropic LC polyester BB-8 (Scheme 1), synthesized from dimethyl *p*,*p*′-bibenzoate and octamethylenediol, is a well-known thermotropic LC polymer whose properties have been studied in detail for these 20 years.[11–14] Previous thermal analysis of BB-8 revealed that this LC polymer forms the isotropic, smectic A, and crystalline phases in the order of decreasing temperature.[12] The conformation of the CH_2 sequences of BB-8 in the noncrystalline component, corresponding to the supercooled smectic A component, should be clarified for comparison with that of the supercooled nematic component for the LC polyurethane (UDMB-10) or polyether (EDMB-10). The smectic A phase has more ordered structure than the nematic phase, and thus conformation of the CH_2 sequences in BB-8 may be more restricted even in the noncrystalline region.

This paper applies a similar solid-state ^{13}C NMR analytical method previously used for other LC polymers to the BB-8 sample, crystallized from the melt through the smectic A phase, and characterizes the crystalline–noncrystalline structure and dynamics, particularly paying attention to the conformation and molecular motion of the mesogen and spacer units in the respective components.

EXPERIMENTAL

Sample

Thermotropic liquid crystalline polyester BB-8 was synthesized by melt transesterification of dimethyl *p*,*p*′-bibenzoate and octamethylenediol with isopropyl titanate as catalyst.[13,14] The inherent viscosity was 1.00 dL/g, as measured at 30 °C in a 60/40 w/w mixture of phenol and tetrachloroethane. The sample obtained was crystallized under an argon atmosphere by cooling from the melt at 210 °C through the smectic A phase at a rate of 1 °C/min.

Differential Scanning Calorimetry (DSC)

Thermal transition behavior was studied by a TA Instruments DSC 2910 differential scanning calorimeter. Indium was used as a standard for temperature calibration. All DSC measurements were carried out under nitrogen atmosphere with sample amount of 4.4 mg. First-order phase transition temperatures were determined from maxima or minima of the endothermic or exothermic peaks, respectively.

Solid-State ^{13}C NMR Measurements

Solid-state ^{13}C NMR measurements were conducted at room temperature on a Chemagnetics CMX 200 spectrometer equipped with a JEOL CP/MAS probe operating at 50.0 MHz under a static magnetic field of 4.7 T.[6–8,15–18] ^1H and ^{13}C radio-frequency fields $\gamma B_1/2\pi$ were 62.5 kHz in the cross polarization (CP) process and the ^1H decoupling field strength was reduced by about 10%. The contact time for CP was 1 ms and the recycle time after acquisition of a free induction decay (FID) was 5 s throughout this work. MAS rate was set at 3.8 kHz to avoid the overlapping of spinning sidebands on other resonance lines. ^{13}C chemical shifts were expressed as values relative to tetramethylsilane (Me_4Si) by using the CH_3 line at 17.36 ppm of hexamethylbenzene crystals as an external reference. ^{13}C spin–lattice relaxation times (T_1^C) were measured using the CPT1 pulse sequence.[19]

Two-dimensional (2D) magic angle turning (MAT) experiments were performed on a Chemagnetics CMX-400 spectrometer operated under a static magnetic field of 9.4 T. ^1H and ^{13}C field strengths $\gamma B_1/2\pi$ of 62.5 kHz, a CP time of 2 ms, an acquisition time of 2.56 ms, a dwell time of 10 μs were used. A triple-echo sheared MAT pulse sequence[20,21] was used in this work. τ delay for the triple Hahn echoes was 20 μs. In the t_1 dimension, 64 slices with increments of 30 μs were acquired. MAS rare was precisely set to 130 ± 1 Hz.

RESULTS AND DISCUSSION

Thermal Transition Behavior

Figure 1 shows DSC thermograms for BB-8 in the cooling process from the isotropic melt at cooling rates of 1–20 °C/min. Two exothermic peaks clearly appeared at all cooling rates examined, in good accord with previous results.[22] The sharper peak observed at a higher temperature corresponds to the transition from the isotropic melt to the smectic A phase and the broader one at a lower temperature the transition from the smectic A phase to the crystalline phase.[22] The liquid crystallization temperature (T_{lc}) is slightly dependent on the cooling rate while the crystallization temperature (T_c) rapidly decreases with increasing cooling rate. Similar cooling rate dependencies of T_{lc} and T_c were observed for LC polyether associated with the nematic phase.[8] In contrast to cooling, it is

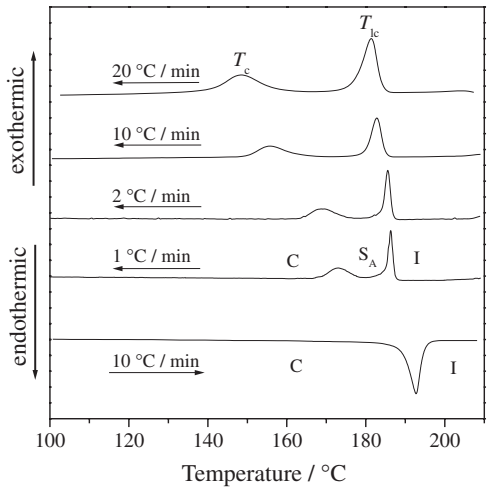

Figure 1. DSC thermograms of BB-8 on cooling and heating at scanning rates of 1–20 °C/min. C, S_A, and I represent the crystalline, smectic A and isotropic phases, respectively. T_c and T_{lc} denote the crystallization and liquid crystallization temperatures, respectively.

difficult to observe separately two corresponding endothermic peaks at any heating rate, as seen in the thermogram at the bottom of Figure 1. This system should be thus assigned to the monotropic LC polymer system.[3]

CP/MAS ^{13}C NMR Characterization

First we have characterized the crystalline–noncrystalline structure of the BB-8 sample, crystallized by cooling from the isotropic melt to room temperature through the smectic A phase at a rate of 1 °C/min in a silicone bath, by CP/MAS ^{13}C NMR spectroscopy. Figure 2 shows the CP/MAS ^{13}C NMR spectrum of the sample measured at room temperature. Except for C7–C9 CH_2 carbons, assignments of resonance lines were made on the basis of assignments in solution performed by H–H COSY and conventional or long-range C–H COSY experiments. Quaternary and protonated carbon lines for the mesogen group were discriminated by dipolar dephasing. Resonance lines at 36–30 ppm were assigned to the respective CH_2 carbons, as described later in detail, by considering the *γ-gauche* effect[23] on ^{13}C chemical shift values. Although the respective lines do not explicitly split into the crystalline and noncrystalline lines unlike polyethylene or polypropylene samples isothermally crystallized,[16,17] these lines will contain real contributions from both crystalline and noncrystalline regions. To separately obtain spectra of the respective components for the BB-8 sample in a similar way for other crystalline polymers,[16–18] ^{13}C spin–lattice relaxation was measured for this sample at room temperature by the CPT1 pulse sequence.[19]

In Figure 3, the logarithmic peak intensity of the C8 resonance line at 30.9 ppm is plotted against the relaxation decay time τ in the CPT1 pulse sequence. The experimental decay curve designated as filled circles appears not to be described by a single exponential and thus the decay was resolved into plural expo-

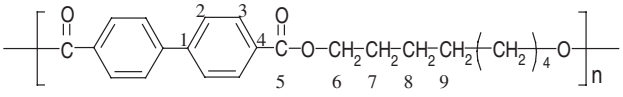

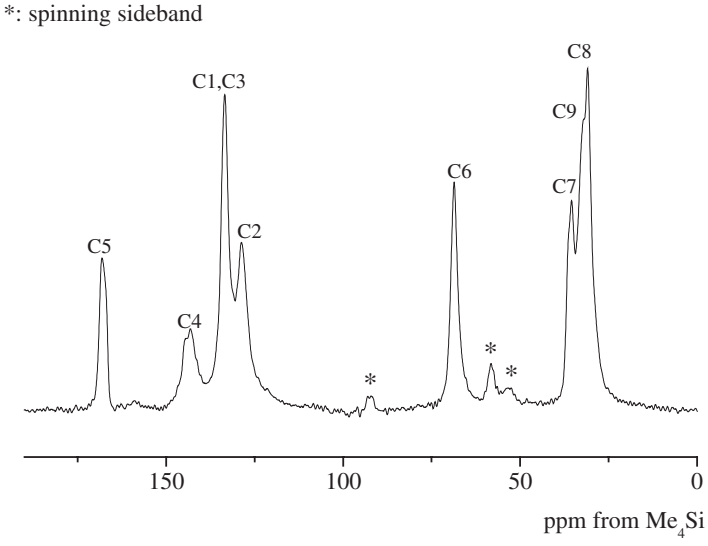

Figure 2. CP/MAS ^{13}C NMR spectrum of the BB-8 sample crystallized from the melt through the smectic A phase, measured at room temperature. * indicates a spinning sideband.

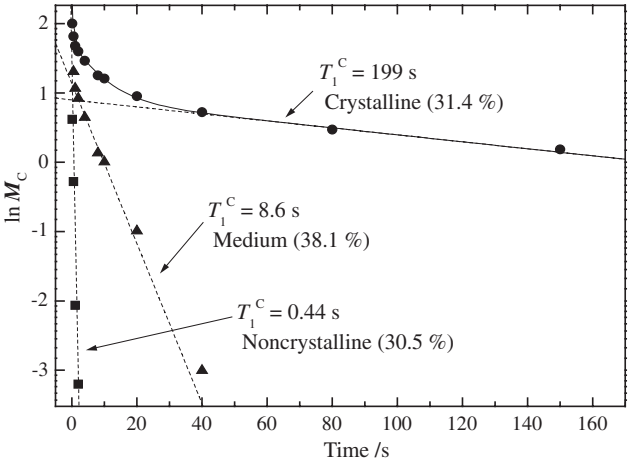

Figure 3. ^{13}C spin–lattice relaxation for the C8 resonance line measured at room temperature for the BB-8 sample by the CPTl pulse sequence.

nentials having different T_1^Cs by the computer-aided nonlinear least-squares method as carried out for other crystalline and LC polymers.[6–8,10,15–18] The decay curve is found to be well described in terms of three components with $T_1^C = 199$, 8.6, and 0.44 s, which are separately described by broken lines in this figure. For reference, percentages of the components are shown in the figure, although the values may not exactly indicate real mass fractions because of differences in CP efficiency. Similar analysis was carried out for other resonance lines and the T_1^Cs obtained are compiled in Table I.

All carbons of the mesogen and spacer units have three T_1^Cs of 200–430, 9–38, and 0.4–5.5 s, suggesting clear phase separation into the crystalline and noncrystalline regions. Since the longer T_1^C is associated with the less molecular mobility under this experimental condition, the components with longest and shortest T_1^C should be attributed to the crystalline and noncrystalline components, respectively. Wide-angle X-ray diffraction also indicates the presence of the crystalline region in the BB-8 sample.[22,24] The noncrystalline component may correspond to the supercooled smectic A component, because crystallization occurs through the smectic A phase from the melt and some part may be left as noncrystalline component after crystallization. Similar supercooled LC components were observed for the UDMB-10 and EDMB-10 samples crystallized through the nematic phase from the isotropic melt.[6–8] In contrast, assignment of the component with intermediate T_1^C values cannot be readily made at present, although this component may be an interfacial component between the crystalline and noncrystalline components,[25] and thus simply called the medium component.

Conformation of the Spacer CH_2 Sequences and Mesogen Groups in Each Component

The T_1^Cs of the crystalline, medium, and noncrystalline components are markedly different and thus we can separately record their high-resolution ^{13}C NMR spectra as follows: The spectrum of the crystalline component has been selectively measured using the CPT1 pulse sequence[19] by setting T_1^C decay time τ to 100 s. The spectrum of the medium component was obtained by subtracting the crystalline spectrum from the spectrum measured by the CPT1 pulse sequence with $\tau = 3$ s. The noncrystalline component spectrum was measured by the saturation recovery method modified for solid-state measurements[25] by setting the recovery time τ_r to 0.3 s. The background from the probe materials appearing in this case was subtracted using the blank measurement. Figure 4 shows the high-resolution ^{13}C NMR spectra of the crystalline, medium, and noncrystalline components obtained in the CH_2 carbon region. The results of line shape analysis are also shown as broken lines in the figure, as obtained assuming each constituent line a Lorentzian curve. In Table II, ^{13}C chemical shift values are summarized for the lines in each component obtained by line shape analysis. Relative intensities of the respective lines are not exactly proportional to compositional ratios of the corresponding carbons because T_1^Cs associated with the intensity are significantly different in the respective lines.

As clearly seen in Figure 4a and b, chemical shifts of the CH_2 carbons for the crystalline and medium

Table I. ^{13}C spin–lattice relaxation times (T_1^C) of the spacer and mesogenic carbons in the respective components at room temperature for BB-8

Component	T_1^C/s						
	Mesogen				Spacer		
	qC[a] C4	qC,[a,b] CH[b] C1, C3	CH C2	CO C5	CH_2 C7	CH_2 C8	CH_2 C9
Crystalline	305	282	294	427	196	199	163
Medium	23.0	14.9	12.6	37.5	13.5	8.60	8.25
Noncrystalline	1.32	0.50	0.49	5.46	0.53	0.44	0.48

[a]qC denotes a quaternary carbon. [b]Overlapping signals.

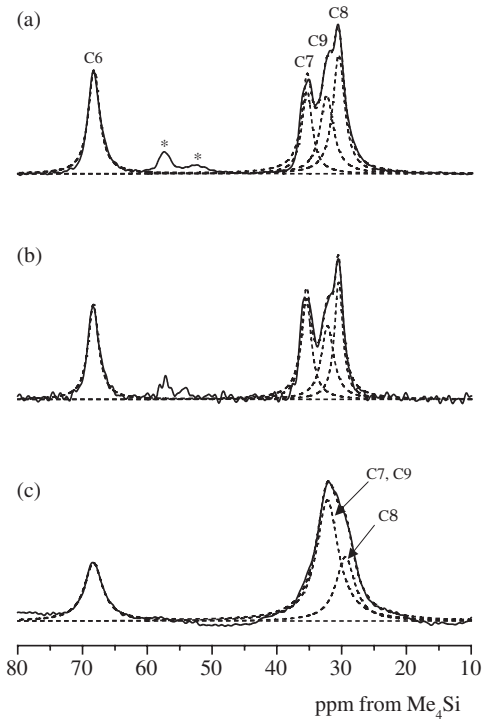

Figure 4. Line shape analysis for CH_2 resonance lines of different components in the BB-8 sample: (a) crystalline, (b) medium, (c) noncrystalline.

Table II. ^{13}C isotropic chemical shifts (δ_{iso}) of the spacer and mesogen carbons obtained by the lineshape analysis for components of BB-8 samples

Carbon	δ_{iso}/ppm		
	Crystalline	Noncrystalline	Solution
Spacer			
C6	68.2 (−2.0)	68.3 (−2.1)	66.2
C7	35.3 (−6.8)	32.2 (−3.7)	28.5
C8	30.4 (−4.6)	29.4 (−3.6)	25.8
C9	32.3 (−3.3)	32.2 (−3.2)	29.0
Mesogen			
C1	133.2 (+3.9)	132.8 (+2.8)	129.3
C2	128.2 (+1.1)	128.6 (+1.5)	127.1
C3	133.2 (+3.2)	132.8 (+2.8)	130.0
C4	144.3 (+0.1)	143.9 (−0.3)	144.2
	142.6 (−1.6)		
	140.9 (−3.3)		
C5	168.1 (+0.1)	167.7 (−0.3)	168.0
	166.5 (−1.5)		

Values in parentheses for the carbons in each sample are differences in chemical shifts between each component and solution measured at 60 °C.

components are in good accord with each other within an experimental error. This indicates that the chain conformations are the same for these two components. In contrast, C7–C9 resonance lines of the noncrystalline component are rather broader and, more importantly, some line seems to appreciably shift upfield. This suggests that the spacer CH_2 sequences adopt another chain conformation in the noncrystalline component while these sequences have the all-*trans* conformation in the crystalline region as confirmed for BB-6, composed of six CH_2 spacer sequences and the same mesogen groups, by wide-angle X-ray diffractometry.[26–28]

Before evaluation of the chain conformation of the noncrystalline component, the assignment of the C7–C9 resonance lines should be established first for the crystalline component by comparing their chemical shifts with those in solution. The C8 resonance line appears at 25.8 ppm in solution as seen in Table II. Although the CH_2 sequences adopt the all-*trans* conformation in the crystalline region similarly to the case of BB-6,[26–28] almost all C–C bonds may have the *trans–gauche* exchange conformation in solution for BB-8. When the *trans–gauche* exchange conformation is introduced to C6–C7 and C9–C9 bonds in solution, the C8 line may shift 5–6 ppm upfield in solution compared to the line in the crystalline state due to the *γ-gauche* effect.[23] Here, it is assumed that the *γ-gauche* effect induces 5–6 ppm upfield shift[23] and thus one C–C bond with the *trans–gauche* exchange conformation produces 2.5–3 ppm upfield shift which corresponds to half the normal *γ-gauche* effect. Therefore, the resonance line at 30.4 or 32.3 ppm for the crystalline component is ascribed to the C8 carbon. If the line at 32.3 ppm could be assigned to the C8 carbon, the line at 30.4 ppm would be attributed to the C9 carbon. However, the *trans* conformation must be introduced to the C7–C8 and C8–C9 bonds in this case even in solution, because almost no difference in chemical shift appears between the crystalline and dissolved states. This should not be the case. Further evaluation of the CH_2 sequence for the noncrystalline component becomes impossible when the line at 30.4 ppm is assumed to be the C7 carbon. Thus resonance lines at 30.4, 32.3, and 35.3 ppm for the crystalline component are assigned to the C8, C9, and C7 carbons, respectively. ^{13}C chemical shifts of the respective lines thus assigned are shown in Table II.

On the basis of the assignments established for the crystalline component, the chain conformation of the noncrystalline component is evaluated as follows: The line shape analysis of this component shown in Figure 4c indicates that the broad CH_2 resonance lines at about 30 ppm consist of two constituent lines at 32.2 and 29.4 ppm with different intensities. Their chemical shifts are in good accord with those of the C9 and C8 carbons for the crystalline component, as seen in Table II. It is thus plausible to assign the downfield and upfield lines to the C7/C9 and C8 carbons for the noncrystalline components, respectively. According to this assignment, the C7 resonance line

Crystalline, Medium

6 7 8 9 9 8 7 6

-O-CH_2-CH_2-CH_2-CH_2-CH_2-CH_2-CH_2-CH_2-O-

t t t t t t t t t

Noncrystalline

-O-CH_2-CH_2-CH_2-CH_2-CH_2-CH_2-CH_2-CH_2-O-

x t t t t t t t x

Figure 5. Chain conformation of the spacer CH_2 sequence for each component in the BB-8 sample. *t* and *x* indicate *trans* and *trans–gauche* exchange conformations, respectively.

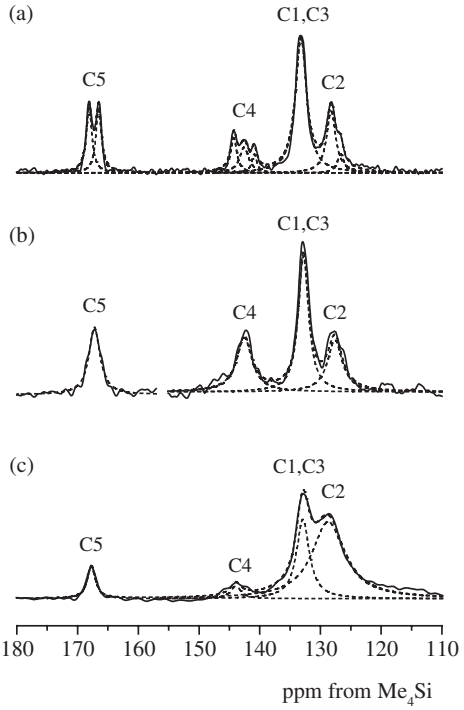

Figure 6. Line shape analysis for the resonance lines of the mesogen units for different components in the BB-8 sample: (a) crystalline, (b) medium, (c) noncrystalline.

evidently shifts about 3 ppm upfield compared to the C7 line for the crystalline component. This indicates that the *trans–gauche* exchange conformation is introduced to either the C8–C9 bond or the C6–oxygen bond in the noncrystalline component. If the former happens, the C9 line would be also subjected to 2.5–3 ppm downfield shift as a result of half the *γ-gauche* effect. Since this is not the case, it can be concluded for the noncrystalline component that the C6–oxygen bond adopts the *trans–gauche* exchange (*x*) conformation while other C–C bond of the CH_2 sequences have the *trans* conformation.[29] Figure 5 shows the spacer conformation thus clarified for the noncrystalline component together with the all-*trans* conformation for the crystalline and medium components.

Figure 6 shows high-resolution ^{13}C NMR spectra of the mesogen units of the crystalline, medium, and noncrystalline components. The spectrum of the crystalline component was selectively measured by the CPT1 pulse sequence[19] with $\tau = 100$ s and the spectrum for the medium component was obtained by subtracting the crystalline spectrum from the spectrum measured by the CPT1 pulse sequence with $\tau = 30$ s for the carbonyl carbons or with $\tau = 10$ s for the phenylene carbons. The noncrystalline component spectrum was selectively measured by the saturation recovery method modified for solid-state measurements[25] by setting the recovery time to 2 s. In the latter case the background from the probe materials was subtracted by blank measurement. The results of the line shape analysis for each component, obtained by assuming the respective lines to be Lorentzians, are shown as broken lines in the figure. ^{13}C chemical shifts determined as peak tops for the respective lines are summarized in Table II.

C5 and C4 resonance lines of the crystalline component split into two and three lines, respectively, as seen in Figure 6a. The cause for this is not understood at present but, according to the previous solid-state NMR measurements and quantum chemistry calculations,[30,31] chemical shifts of the biphenyl carbons markedly depend on the dihedral angle around the bond axis of the two benzene rings. In the case of LC polyether composed of similar biphenyl groups, notably systematic upfield shifts were observed for biphenyl carbons in the crystals called as form *α* compared to those in the melt. Thus, co-planarity of each biphenyl group is much higher in the crystalline region than in the melt.[10] In contrast, chemical shifts of C1–C4 carbons of the biphenyl groups in BB-8 seem to undergo significant downfield shift compared to those in solution as seen in parentheses in Table II. This suggests that the co-planarity of the biphenyl groups may be much less in the crystalline region than in solution for BB-8. The dihedral angle of the biphenyl groups for BB-6 was determined to be 40° in the most stable crystalline form by wide-angle X-ray diffractometry.[27] However, C4 carbons are exceptionally subjected to appreciable upfield shift, as seen in Table II, and this may be due to another effect of the co-planarity between the carbonyl and neighboring phenylene groups. The doublet of the carbonyl (C5) carbons may thus indicate the existence of two dihedral angles around the C4–C5 bonds in the crystalline region. C4 resonance line may split into two lines but additional effect associated with the dihedral angle around the C1–C1 bond in the biphenyl unit may induce additional splitting. Such effects probably induce triplet splitting for the C4 carbons. A small upfield contribution of the C2 carbons may partly ex-

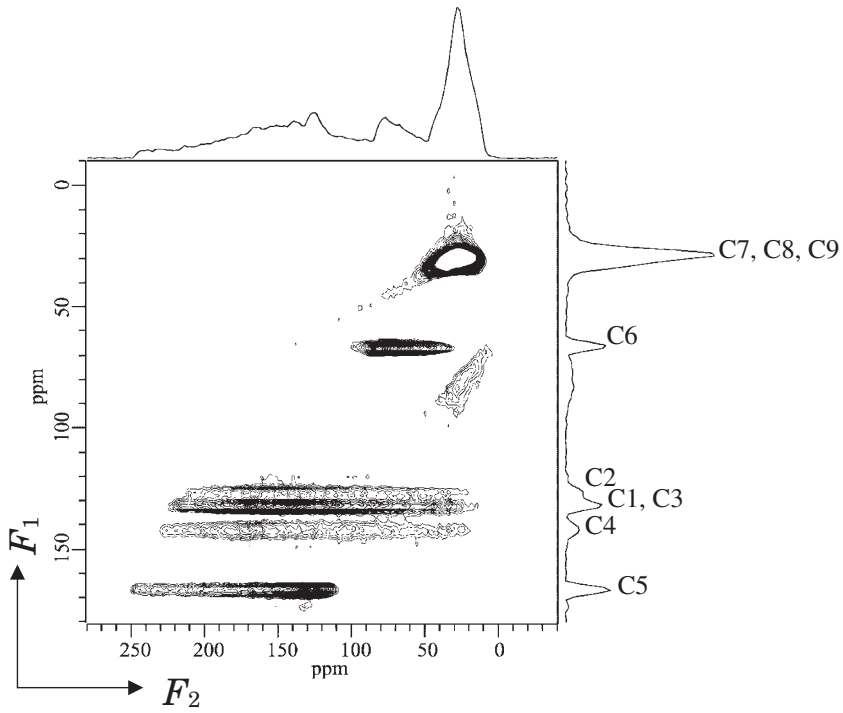

Figure 7. 2D MAT ^{13}C NMR spectrum measured at room temperature for the BB-8 sample.

plain the triplet. More detailed characterization will be made by advanced solid-state NMR spectroscopy and wide-angle X-ray diffractometry.

Medium and noncrystalline component chemical shifts of the mesogen carbons are in good accord with each other, indicating almost the same structure for the mesogen groups in these two regions although the structural distribution is much wider in the noncrystalline region than in the medium region. In particular, the chemical shifts of the C4 and C5 carbons for the medium and noncrystalline components are nearly equal to those in solution. The carbonyl and phenylene groups may thus be almost coplanar in the medium and noncrystalline components as well as in solution probably due to molecular motion around the C4–C5 bond.

Molecular Motion of the Mesogen and Spacer Units

As seen in Table I, $T_1{}^C$s of the mesogen aromatic carbons are 280–300 s for the crystalline component. This indicates that the mesogen groups in this component are highly inhibited in molecular mobility on a time scale of 10^{-8} s associated with the $T_1{}^C$ relaxation. In contrast, corresponding $T_1{}^C$s are greatly reduced to 0.5–1.3 s for the noncrystalline component. This suggests that the phenylene rings may undergo so-called 180° flip motion or random fluctuation with relatively large amplitudes around the phenylene axis in this component. To examine molecular motion of the mesogen groups in detail, the ^{13}C CSA spectrum for each carbon was measured in the same way as for other LC polymers[7,8,10] by 2D MAT.[20,21]

Figure 7 shows the 2D MAT spectrum measured for the BB-8 sample at room temperature. "Sky projection" plots of the highest points in each row or column for the 2D spectrum are shown along the F_2 or F_1 axis, respectively. The high resolution spectrum without sidebands, which corresponds to the CP/MAS spectrum with sidebands shown in Figure 2, is obtained as the "sky projection" plot in the F_1 dimension at the right side of the figure. The CSA spectra can be successfully obtained in this sample along the F_2 axis for the respective ^{13}C resonance lines in the high resolution projection spectrum.

Figure 8 shows the CSA spectra thus obtained as slices along the F_2 axis for respective ^{13}C species. Their line shapes may reflect the local electronic environment which significantly differs in the respective carbons. The CSA spectra theoretically simulated in the rigid state are shown as broken lines for the mesogen and carbonyl carbons. Except for overlapped C1 and C3 CSA spectra, the observed CSA spectra are in good accord with the simulated spectra for the C4 and C5 carbons not directly associated with the phenylene flip motion. In contrast, the discordance seems appreciably large for the C2 carbon. Such discordance may be produced from the noncrystalline contribution and thus subtraction of the rigid CSA spectrum from the observed CSA was performed by considering relative intensities of the crystalline and two other components obtained by $T_1{}^C$ relaxation measurements. Figure 9 shows the subtracted CSA spectrum obtained

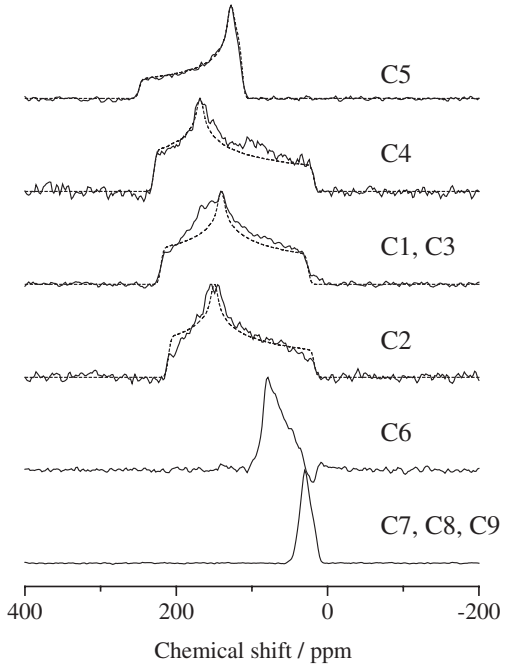

Figure 8. CSA spectra for different carbons in the BB-8 sample, obtained as slices along the F_2 axis in the 2D MAT spectrum shown in Figure 7. Broken lines are the CSA powder patterns simulated for the respective carbons in the rigid state.

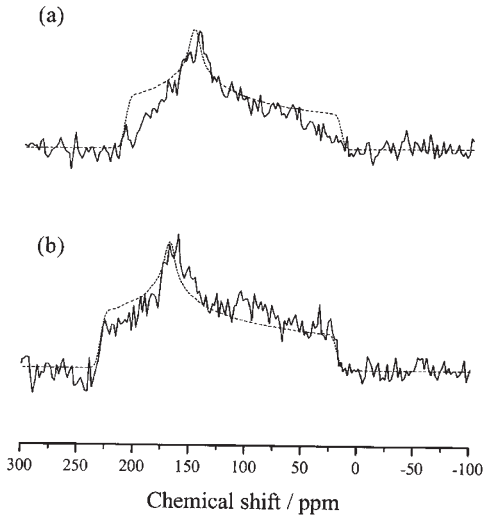

Figure 9. ^{13}C CSA total spectra of medium and noncrystalline components obtained by subtraction of the rigid spectra from the observed spectra. (a) C2 carbon, (b) C4 carbon.

for the C2 carbon together with the corresponding spectrum for the C4 carbon for reference. These CSA spectra reflect total contributions from the medium and noncrystalline components. The C2 CSA spectrum undergoes much narrowing compared to the rigid spectrum designated as a broken line while the C4 spectrum is not significantly different from the rigid spectrum. This indicates that phenylene groups are mainly subjected to rapid fluctuation around the C1–C4 axis which may induce fast T_1^C relaxation of the medium and noncrystalline components. Nevertheless, the C2 line shape could not be well reproduced by the two-site flip motion of the phenylene ring at any flip angle and frequency.[10] Since the σ_{33} contribution seems to appreciably narrow, the C1–C4 axis may also undergo restricted fluctuation with rather small amplitudes to induce only minor change in CSA for the C4 carbon. Similar but much lower molecular mobility of the phenylene rings was confirmed for the noncrystalline component in the EDMB-10 sample by our recent analysis.[32] Since such phenylene motion is highly restricted even in the noncrystalline region for the UDMB-10 sample,[32] intermolecular interaction such as hydrogen bonding is closely associated with molecular mobility of the phenylene groups. However, much higher molecular mobility in the noncrystalline region for the BB-8 sample suggests that phenylene fluctuation may more preferably occur in the smectic A phase than in the nematic phase.

Principal values σ_{11}, σ_{22}, σ_{33} of the chemical shift tensor used in the simulations of the rigid CSA spectra are compiled in Table III. For comparison, the corresponding values for dimethoxy benzene (DMB) and diethoxy benzene (DEB) crystals[33] as well as for poly(ethylene terephthalate) (PET)[34] are given in this table. Chemical shift anisotropy $|\sigma_{11} - \sigma_{33}|$ of the aromatic CH carbon for the BB-8 sample seems not

Table III. Principal values of ^{13}C chemical shift tensors for mesogenic and carbonyl carbons obtained by the magic angle turning method

Sample	Carbon	Chemical shift/ppm				
		σ_{11}	σ_{22}	σ_{33}	$\lvert\sigma_{11} - \sigma_{33}\rvert$	σ_{iso}[a]
BB-8	C1 (qC[b]), C3	216	142	34	182	133
	C2 (CH)	212	155	17	195	128
	C4 (qC)	231	171	21	210	143
	C5 (CO)	248	127	117	131	167
DMB[c]	qC	243	160	71	172	158
	CH	199	137	22	177	119
	CH	194	131	13	181	113
DEB[d]	qC	233	160	71	162	155
	CH	199	135	24	175	119
	CH	194	129	11	183	111
PET[e]	CH	223	158	13	210	131
	qC	228	146	31	197	135
	CO	252	126	113	139	164

[a]Determined by the MAS experiment for BB-8. Others were calculated from the principal values. [b]qC denotes a quaternary carbon. [c]dimethoxy benzene (ref 33) [d]diethoxy benzene (ref 33) [e]ref 34

much different from values for DMB and DEB crystals. This confirms that the phenylene rings in the mesogen units may be highly hindered in molecular motion in the crystalline component as expected.

The CSA spectrum of the C6 (OCH_2) carbon shown in Figure 8 seems xially symmetric as with LC polyurethane and polyether[7,8,10] and the chemical shift anisotropy $|\sigma_{11} - \sigma_{33}|$ is also of the same order for the corresponding carbons in the latter samples.[7,8,10] σ_{11} and σ_{22} of the OCH_2 carbons in the rigid state are equal to each other for poly(ethylene terephthalate)[33,35] or not so greatly different for poly(ethylene oxide).[33,36] Accordingly, it is difficult to obtain information on the molecular motion of OCH_2 carbons from CSA line shape.

The slice CSA spectrum of C7–C9 carbons in the spacer unit in Figure 7 seems to narrow to a considerable extent reflecting the higher molecular mobility of the CH_2 sequences. Figure 10 shows the enlarged spectrum of the CH_2 carbons together with the CSA powder spectrum having the same isotropic chemical shift for the CH_2 carbon in the rigid state. The latter spectrum was simulated using the principal values for polyethylene crystals.[33,37] Although the contributions of the three constituent CH_2 carbons are involved in the observed CSA spectrum, the overall spectrum narrows to a significant extent. Such narrowing should be a reflection of random fluctuation around the energy minimum of the *trans* conformation for the CH_2 sequences in the crystalline region. The same effect of the molecular motion on the CSA lineshape seems to be given to the noncrystalline component, although the conformation of the CH_2 sequence is appreciably different from the all-*trans* conformation in the crystalline region.

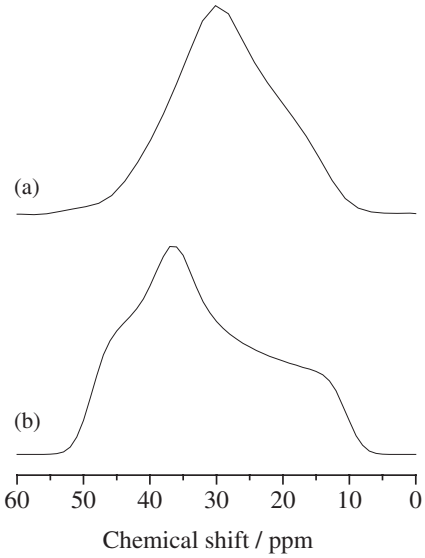

Figure 10. (a) Enlarged CSA spectrum of the C7–C9 carbons originally shown in Figure 8. (b) CSA powder spectrum for polyethylene crystals with an isotropic chemical shift value of 32.4 ppm.

Molecular Structure Model

In the noncrystalline component, conformations of the CH_2 sequences are more restricted for the BB-8 sample than other LC polymers, UDMB-10 and EDMB-10,[6–8,10] as seen in Figures 6 and 11; only the O–C bond adopts the *trans–gauche* exchange (*x*) conformation while all remaining C–C bonds are in the *trans* (*t*) conformation. In contrast, alternative exchange or all-exchange conformation, indicated as *ttxtxtxtt* for UDMB-10, *xxxxxxxxx* or $t'xxxxxxxt'$ for EDMB-10, is allowed for the latter polymers. Such difference in the spacer conformation may be mainly due to the structure difference between the smectic A and nematic phases because the noncrystalline component of each LC polymer corresponds to the component super-cooled from the LC phase. Since the smec-

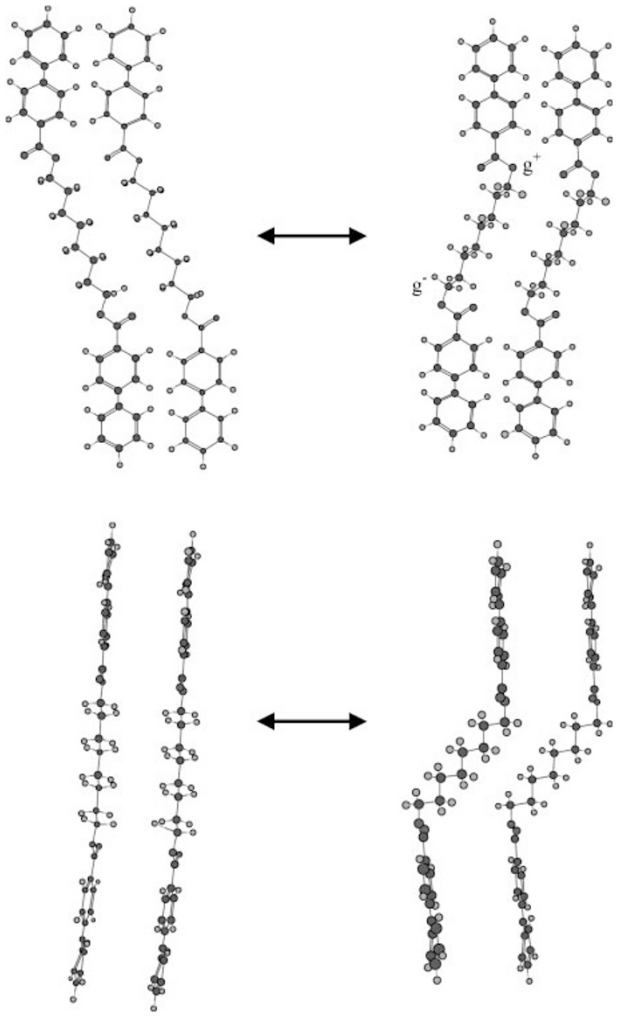

Figure 11. Schematic representation for the *trans–gauche* exchange motion proposed for the spacer CH_2 sequence of the noncrystalline component in the BB-8 sample.

tic A phase has a layer structure, the spacer conformation or molecular mobility may be more restricted in this phase than that in the nematic phase.

In Figure 11, a molecular structure model is proposed for the spacer conformation in the noncrystalline region, which corresponds to the supercooled smectic A phase, for BB-8. O–C bonds have the *trans* (*t*) or *gauche* (*g*) conformation and *t* and *g* are rapidly exchangeable (*x*). In this case, when a pair of *gauche*$^+$ (g^+) and *gauche*$^-$ (g^-) are introduced to the two O–C bonds at the ends of the spacer CH_2 sequence, almost no change in orientation occurs for the mesogen units compared to the case of the *trans* conformation as seen in Figure 11 although some translational displacement occurs for the units. Such cooperative exchange motion is preferably allowed in the smectic A phase because the structural features of this phase seem not to be disturbed by the motion. Such translational motion of the mesogen units may induce rapid fluctuation of the phenylene rings around the bond axis as well as minor fluctuation of the axis itself, resulting in appreciable CSA narrowing in good accord with the experimental observation described above.

Acknowledgment. This work was supported by Grant-in-Aid for Scientific Research (No. 12450384) from the Ministry of Education, Culture, Sports, Science and Technology, Japan.

REFERENCES

1. A. Ciferri, Ed., "Liquid Crystallinity in Polymers. Principles and Fundamental Properties," VCH Publishers, New York, N.Y., 1991.
2. A. I. Isayev, T. Kyu, and S. Z. D. Cheng, Ed., "Liquid-Crystalline Polymer Systems. Technological Advances," ACS Symp. Series 632, American Chemical Society, Washington, D.C., 1996.
3. P. J. Collings and J. S. Patel, Ed., "Handbook of Liquid Crystal Research," Oxford University Press, New York, N.Y., 1997.
4. I. M. Ward, Ed., "Structure and Properties of Oriented Polymers," Chapman & Hall, London, U.K., 1997.
5. T.-S. Chung, Ed., "Thermotropic Liquid Crystal Polymers," Technomic Publishing, Lancaster, PA, 2001.
6. H. Ishida, H. Kaji, and F. Horii, *Macromolecules*, **30**, 5799 (1997).
7. H. Ishida, H. Kaji, and F. Horii, *Macromolecules*, **34**, 7751 (2001).
8. M. Murakami, H. Ishida, M. Miyazaki, H. Kaji, and F. Horii, *Macromolecules*, **36**, 4160 (2003).
9. M. Murakami, H. Ishida, H. Kaji, and F. Horii, *Polym. J.*, **35**, 951 (2003).
10. M. Murakami, H. Ishida, H. Kaji, and F. Horii, *Polym. J.*, **36**, 403 (2004).
11. J. Watababe, M. Hayashi, Y. Nakata, and M. Tokita, *Prog. Polym. Sci.*, **22**, 1053 (1997).
12. J. Watababe and M. Hayashi, *Macromolecules*, **21**, 278 (1988).
13. W. R. Krigbaum and J. Watanabe, *Polymer*, **24**, 1299 (1983).
14. W. R. Krigbaum, J. Asrar, H. Toriumi, A. Ciferri, and J. Preston, *J. Polym. Sci., Polym. Lett. Ed.*, **20**, 109 (1982).
15. H. Ishida and F. Horii, *Macromolecule*, **35**, 5550 (2002).
16. K. Kuwabara, H. Kaji, F. Horii, D. C. Bassett, and R. H. Olley, *Macromolecule*, **30**, 7516 (1997).
17. Y. Ohira, F. Horii, and T. Nakaoki, *Macromolecules*, **34**, 1655 (2001).
18. K. Masuda and F. Horii, *Macromolecules*, **31**, 5810 (1998).
19. D. A. Torchia, *J. Magn. Reson.*, **30**, 613 (1978).
20. Z. Gan, *J. Am. Chem. Soc.*, **114**, 8307 (1992).
21. J. Z. Hu, A. M. Orendt, D. W. Alderman, R. J. Pugmire, C. Ye, and D. M. Grant, *Solid State Nucl. Magn. Reson.*, **3**, 181 (1994).
22. M. Tokita, K. Osada, and J. Watanabe, *Liq. Cryst.*, **23**, 453 (1997).
23. A. E. Tonelli, "NMR Spectroscopy and Polymer Microstructure: The Conformational Connection," VCH Publishers, New York, N.Y., 1989.
24. M. Tokita, K. Osada, and J. Watanabe, *Polym. J.*, **30**, 589 (1998).
25. R. Kitamaru, F. Horii, and K. Murayama, *Macromolecules*, **19**, 636 (1986).
26. J. Watababe and M. Hayashi, *Macromolecules*, **22**, 4083 (1989).
27. X. Li and F. Brisse, *Macromolecules*, **27**, 7725 (1994).
28. In the case of BB-6, there are three crystal forms, α, β, and γ, which are produced by the crystallization or crystal–crystal transformation when slowly cooled from the melt through the smectic A phase and most stable polymorph is form α.[27] In contrast, no crystal–crystal transitions were observed by DSC as seen in Figure 1. Therefore, it may be plausible that only the crystal form corresponding to form α for BB-6 will be produced in the case of BB-8 without any additional crystal–crystal transition.
29. In the Newman's projection along the C6–O bond in this polyester, there are three potential minima around the bond which correspond to *trans*, *gauche*$^+$, and *gauche*$^-$ in the CH_2 sequence. In the text, therefore, it was concluded that the C6–O bond adopts the *trans–gauche* exchange (*x*) conformation, by simply assuming that the CO groups may induce the same level of the γ-*gauche* effect as the CH_2 group. However, since the OH group is known to produce about 2 ppm larger downfield shift as γ-*gauche* effect compared to the case of the CH_2 groups,[23] the CO group may also induce significantly larger γ-*gauche* effect than the CH_2 group. If it is the case for this polymer, the *trans* probability of the exchange conformation will be appreciably increased. Nevertheless, it should be concluded that the C6–O bond basically adopts the *trans–gauche* exchange (x') conformation with a significant *gauche* probability.
30. S. Ando, T. Horonaka, H. Kurosu, and I. Ando, *Magn. Reson. Chem.*, **38**, 241 (2000).
31. D. H. Barich, R. J. Pugmire, D. M. Grant, and R. J. Iuliucci, *J. Phys. Chem. A*, **105**, 6780 (2001).

32. Unpublished work.
33. T. M. Duncan, "A Compilation of Chemical Shift Anisotropies," Farragut Press, Chicago, IL, 1990.
34. B. F. Chemlka, K. Schmidt-Rohr, and H. W. Spiess, *Macromolecules*, **26**, 2282 (1993).
35. P. B. Murphy, T. Taki, B. C. Gerstein, P. M. Henrichs, and D. J. Massa, *J. Magn. Reson.*, **49**, 99 (1982).
36. W. W. Fleming, C. A. Fyfe, R. D. Kendrick, J. R. Lyerla, H. Vanni, and C. S. Yannoni, in "Polymer Characterization by ESR and NMR," A. E. Woodward and F. A. Bovey, Ed., ACS Symp. Series 142, American Chemical Society, Washington, D.C., 1980, p 193.
37. D. L. VanderHart, *J. Chem. Phys.*, **64**, 830 (1976).